XIX IMEKO World Congress
Fundamental and Applied Metrology
September 6–11, 2009, Lisbon, Portugal

AERODYNAMIC LOADS MEASUREMENT OF A SOUNDING ROCKET VEHICLE TESTED IN WIND TUNNEL

Maria Luísa Reis [1], *João Batista Falcão* [2] , *Giuliano Paulino* [3], *Cláudio Truyts* [4]

[1] Institute of Aeronautics and Space, São José dos Campos, Brazil, mluisareis@iae.cta.br
[2] Institute of Aeronautics and Space, São José dos Campos, Brazil, jb.falcao@ig.com.br
[3] São Paulo State University, São Carlos, Brazil, giulianomp@hotmail.com
[4] Institute of Aeronautics and Space, São José dos Campos, Brazil, ctruyts@iae.cta.br

Abstract – In wind tunnels, aerospace vehicle models are tested in order to analyze their performance in real flight situations. The forces and moments exerted by the airflow on the surface of the test article are measured using multi-component balances. The balance measures the aerodynamic loads by using strain-gages. It is calibrated prior to the tests, resulting in the estimation of the parameters of the polynomial mathematical modelling relating the strain-gage readings to the aerodynamic loads. This paper presents the aerodynamic load values acting on a sounding rocket vehicle under test in a transonic aerodynamic facility. The force and moment coefficients and corresponding uncertainties are also estimated. The vehicle was tested in low Mach number conditions, with the airflow being supplied by the injection system. The second stage of the model was fitted with three different fin deflections. The measured quantities are total pressure, static pressure and total temperature of the flow, as well as the strain gage readings supplied by an internal balance. An analysis of the contribution for the uncertainties in the aerodynamic loads revealed that the measurement precision is the dominant component. The intermediate measurement precision of the tests was also considered.

Keywords: metrological reliability, wind tunnel tests, sounding rockets

1. INTRODUCTION

The vehicle SONDA III is a sounding rocket developed by the Brazilian Institute of Aeronautics and Space (IAE). This is a two stage vehicle with a 30 cm diameter second stage, capable of carrying a payload of approximately 100 kg up to an altitude of 600 km. It is one of the sounding rocket family named Sonda, which started with Sonda I, first launched in 1965.

In 1996, the first stage of Sonda III was adapted to receive European experiments onboard. This new single stage vehicle was known as VS-30.

A boosted version, the VSB-30 (fig. 1), which contains the S31 booster motor was developed in 2001.

The Sonda family has been used in scientific missions, to investigate the behavior of biological, chemical and physical systems under weightless conditions and the development of System of Global Positioning Satellite (GPS) technology for space applications.

Fig. 1. The VSB-30 two stage suborbital vehicle.

Although having been successfully launched several times from different launch sites such as *Barreira do Inferno* – Brazil, *Alcantara* – Brazil, *Andoya* – Norway, and *Kiruna* – Sweeden, no Sonda rocket has ever been tested in Brazilian wind tunnels. The data originating from the wind tunnel tests will be important to the prediction of its flight performance and can be compared to the available data.

Experimental tests have recently been carried out in the Pilot Transonic Wind Tunnel of the Institute of Aeronautics and Space (Fig. 2). The aim of the test campaign is to evaluate the aerodynamic loads acting on the test article Sonda III and the pressure distribution on its surface, for further comparison with the theoretical CFD analysis.

The tested models are presented in Fig. 3. Notice the three different fin deflection angles, aligned at 0^o, 2.5^o and 5^o to the longitudinal axis of the body. The purpose of the deflection is to supply a rolling moment to stabilize the flight.

This paper presents the results originating from the transonic wind tunnel using a multi-component internal balance to measure the aerodynamic loads. The aerodynamic forces and moments coefficients are presented, as well as the values of the uncertainties.

ISBN 978-963-88410-0-1

a)

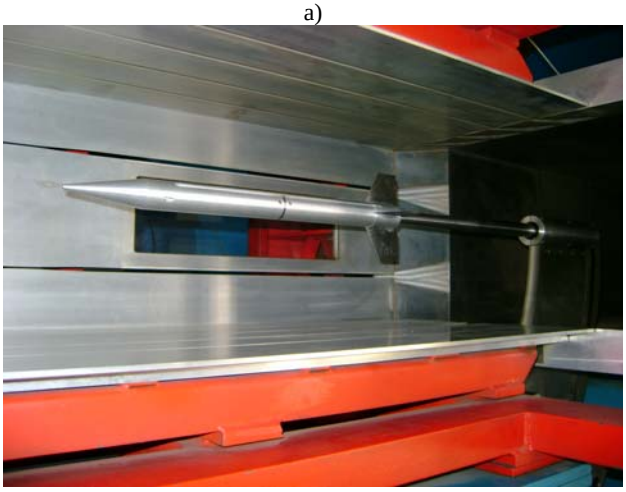

b)

Fig. 2. a) The Pilot Transonic Wind Tunnel facility. b) Sonda III model in the wind tunnel test section.

Fig. 3. The second stage Sonda III models. From left to right, fins at 0°, 2.5° and 5°.

2. THE WIND TUNNEL TEST

Three Sonda III models, with fin deflection angles at 0°, 2.5° and 5°, were tested at nominal Mach number M equal to 0.30, in different configurations of angle of attack α, with the tunnel operating in a closed circuit, driven only by the injection system. Table 1 summarizes the test conditions.

Table 1: wind tunnel test configurations.

Mach number, M	0.30
Reynolds number, Re	1.8×10^5
Angle of attack, α (°)	-10, -8, -6, -4, -2, 0, 2, 4, 6, 8, 10
Fins alignment to the fuselage longitudinal axis	0°, 2.5°, 5°
Fins positioning relating to the test section vertical axis	"+" , "×"

The model was first fixed in the test section with the fins in a crossed position (✣) and afterwards rotated 45° in relation to its longitudinal axis, yielding an "×" configuration (⌘). In the latter position, the auxiliary rails presented on the main body are aligned to the vertical axis of the test section.

The instrument used to measure the aerodynamic loads was an internal aerodynamic balance, whose calibration is performed prior to the test. The methodology of the internal balance calibration is presented in [1].

3. DATA REDUCTION

3.1. Aerodynamic loads

The terminology employed for designating aerodynamic loads in the internal balance calibration process is: axial force (*AF*), side force (*SF*), normal force (*NF*), rolling moment (*RM*), pitching moment (*PM*) and yawing moment (*YM*).

The calibration of the internal balance supplies the parameters a and b of the polynomial which relates the strain gage readings R to the aerodynamic loads (1).

$$F_i = \sum_{j=1}^{6} a_{i,j} R_j + \sum_{j=1}^{6} \sum_{k=j}^{6} b_{i,j,k} R_j R_k \qquad (1)$$

As an example, for the axial force *AF*, Eq. (1) becomes:

$$\begin{aligned} AF = {} & a_{1,1}R_1 + a_{1,2}R_2 + a_{1,3}R_3 + \ldots + a_{1,6}R_6 + \\ & + b_{1,1,1}R_1R_1 + b_{1,1,2}R_1R_2 + \ldots + b_{1,6,6}R_6R_6 \end{aligned} \qquad (2)$$

Due to the variation of the angle of attach α of the Sonda model during the test, the axial and normal forces read by the strain gages must be related to the wind axis. The geometrical relationship between the load components are [2]:

$$\begin{aligned} AF_{wind} &= NF_{balance} \sin\alpha + AF_{balance} \cos\alpha \\ NF_{wind} &= NF_{balance} \cos\alpha - AF_{balance} \sin\alpha \end{aligned} \qquad (3)$$

3.2. Force and moment coefficients

The force coefficients, C_F, and the moment coefficients, C_m, are evaluated through the expressions (4) and (5) respectively:

$$C_F = \frac{F}{qA} \qquad (4)$$

$$C_m = \frac{m}{qAl} \quad (5)$$

where:
F: aerodynamic force (axial, side or normal);
m: aerodynamic moment, (rolling, pitching or yawing);
q: dynamic pressure;
A: reference area; and
l: reference length.

The dynamic pressure in the test section is expressed by

$$q = \frac{1}{2}\rho V^2 \quad (6)$$

where ρ and *V* are the density and the velocity of the flow in the test section at undisturbed conditions (before reaching the model). In this study, the air is considered as a perfect gas. Its density is calculated through:

$$\rho = \frac{p}{RT} \quad (7)$$

p: absolute pressure in pascal;
R: specific gas constant, equal to 287 J/(kg.K) for normal air; and
T: temperature expressed in kelvin.

The reference area used, *A*, which corresponds to the cross sectional area of the fuselage of the model, is equal to 6.2×10^{-4} m^2. The reference length, *l*, corresponds to the diameter of the fuselage, and is equal to 2.8×10^{-2} m^2.

3.3. Mach number

The test results present the aerodynamic coefficients C_F and C_m related to Mach number, *M*. The measured quantities are total pressure p_0, static pressure *p* and stagnation temperature T_0 of the flow, as well as the strain gage readings supplied by the internal balance.

For the estimation of the Mach number, the isentropic relation is used [3]:

$$M^2 = \frac{2}{\gamma - 1}\left[\left(\frac{p_0}{p}\right)^{\frac{(\gamma-1)}{\gamma}} - 1\right] \quad (8)$$

$\gamma = c_P/c_V$: is the ratio of specific heats, equal to 1.4 for air.

The velocity of the flow is evaluated by:

$$V = Ma \quad (9)$$

where *a* represents the speed of sound traveling through the air, considered in this study as a perfect gas. Its value is estimated by:

$$a = \sqrt{\gamma RT} \quad (10)$$

where the static temperature *T* is obtained from the total temperature T_0 by:

$$T = \frac{T_0}{1 + \frac{\gamma - 1}{2}M^2}. \quad (11)$$

3.4. Uncertainty in the force and moment coefficients

The law of propagation of uncertainty is applied to (4) and (5) to estimate the uncertainties in the aerodynamic load coefficients [4]. As an example, for the axial force coefficient:

$$u_{C_{AF}}^2 = \left(\frac{\partial C_{AF}}{\partial AF}\right)^2 u_{AF}^2 + \left(\frac{\partial C_{AF}}{\partial q}\right)^2 u_q^2 + \left(\frac{\partial C_{AF}}{\partial A}\right)^2 u_A^2 \quad (12)$$

which leads to:

$$u_{C_{AF}}^2 = \left(\frac{1}{qA}\right)^2 u_{AF}^2 + \left(\frac{-F}{q^2 A}\right)^2 u_q^2 + \left(\frac{-F}{qA^2}\right)^2 u_A^2 \quad (13)$$

3.5. Reynolds number

The Reynolds number is expressed by [3]:

$$Re = \frac{\rho V l}{\mu} \quad (14)$$

where ρ and *V* are the density and the velocity of the flow in the test section for undisturbed conditions, *l* is the reference length of the model, and the viscosity μ of the flow is based on Sutherland's theory of viscosity [2]:

$$\frac{\mu}{\mu_0} = \frac{(T/T_0)^{\frac{3}{2}}(T_0 + S)}{T + S} \quad (15)$$

μ_0 denotes the viscosity at the reference temperature T_0, and *S* is a constant which for air assumes the value 100 K.

4. RESULTS AND DISCUSSIONS

Data acquisition lasts around 80 s while the injection system takes place. The strain gage readings supplied by the internal balance during the test and the polynomial coefficients evaluated in the internal balance calibration process are the input quantities of (1).

The measurement is controlled by a computer code developed in LabVIEW environment and never starts until the measurement precision [5] of the aerodynamic loads reaches a pre-determined level.

Figure 4 presents the variation with time of the values of the Mach number, total pressure in the injection system and the data reduction of the axial force, *AF*, for one of the tests.

An interval of the temporal series of each aerodynamic component acquisition is chosen according to the stabilization of the signal and the average value of such interval is used for the evaluation of the load coefficients expressed in (4) and (5).

The standard deviation from this interval is computed as well, which represents the dominant component of the uncertainty of the load coefficients (13). The important error

source to the contribution of the experimental data dispersion is the difficulty in supplying a constant flow with the injection system.

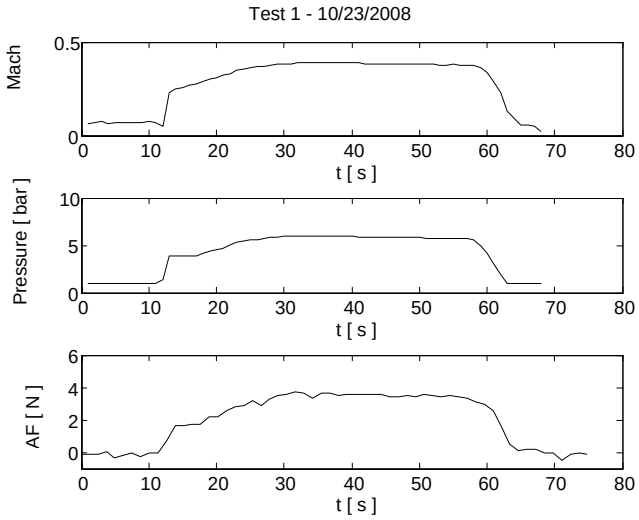

Fig. 4. Mach number *M*, total pressure in the injection system p_0, and axial force component *AF*.

Table 2 presents the mean and standard deviation values of the axial force *AF* for the "+" positioning of the model in the test section. In Figure 5 one can see the correspondent drag coefficient C_{AF} plotted against the angle of attack, for fins at 0°. The estimated uncertainty is also shown. The results are for Mach number of nominal value equal to 0.30.

One can see that the curve in Fig. 5 is not symmetrical in relation to the axis corresponding to the angle of attack equal to zero. The lack of symmetry is due to the presence of the support system of the model, whose structure protrudes into the flow thereby increasing the blockage for negative angles of attack.

Table 2. Data reduction for the axial force *AF*. Unit: Newton.

α (°)	Fins 0 °		Fins 2.5 °		Fins 5 °	
	AF	*S*	*AF*	*S*	*AF*	*S*
-10.0	1.14	0.01	1.13	0.02	1.23	0.01
-8.0	0.92	0.01	0.93	0.01	1.01	0.01
-6.0	0.77	0.01	0.76	0.01	0.86	0.01
-4.0	0.66	0.01	0.68	0.02	0.76	0.01
-2.0	0.61	0.01	0.62	0.01	0.69	0.01
0.0	0.61	0.01	0.63	0.02	0.68	0.01
2.0	0.62	0.02	0.64	0.01	0.70	0.01
4.0	0.68	0.01	0.70	0.01	0.78	0.01
6.0	0.80	0.01	0.81	0.02	0.89	0.02
8.0	0.98	0.01	0.97	0.01	1.06	0.01
10.0	1.20	0.01	1.18	0.01	1.27	0.01

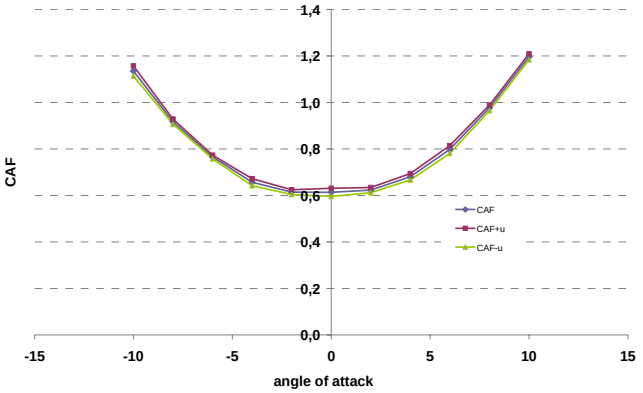

Fig. 5. Drag force coefficient C_{AF} and uncertainty values versus angle of attack.

Figure 6 presents the effect of a spurious side force component C_{SF} resulting in an unexpected yawing moment C_{YM} for model with 0° fin deflection (Fig. 7). For both components, the values should be equal to zero for all ranges of angles of attack considered. This induced side force can arise due to the development of asymmetric vortices caused by manufacturing irregularities of the model. Also, when positioning the model in the wind tunnel, care must be taken in aligning the model in relation to the axis of the wind tunnel test section.

Researchers around the world have been conducting experimental and theoretical studies in order to analyze, explain and correct the error sources that introduce undesirable forces and moments [6]-[11].

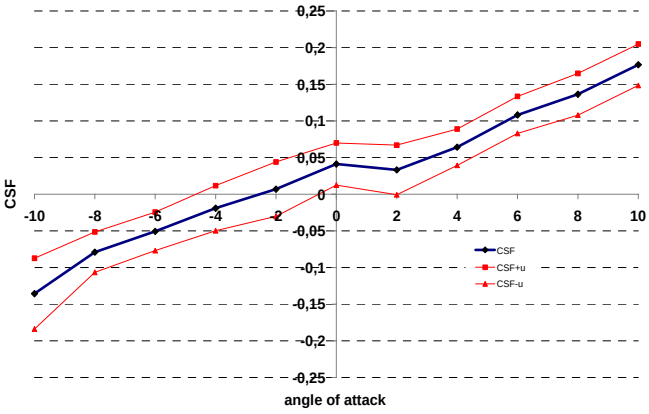

Fig. 6. Unexpected side force component.

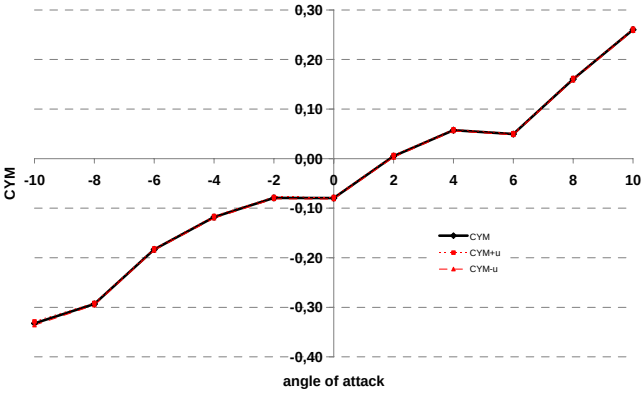

Fig. 7. Yawing moment component induced by error source.

Figure 8 shows the lift coefficient C_{NF}, the drag coefficient C_{AF} and the pitching moment coefficient C_{PM} versus the angle of attack α, for the model Sonda III with fins at 0^o. The uncertainty limits are suppressed for clarity. The center of moment chosen is the internal balance center, which is located 68.5 mm forward from the aft end of the fuselage.

Near $\alpha = 0^o$, the behavior of these aerodynamic load components is as predicted [12]. The lift coefficient C_{NF} changes linearly with the angle of attack. The drag coefficient C_{AF} is approximately proportional to the square of the angle of attack. For the considered range of angle of attack, the pitching moment coefficient C_{PM} also depends linearly on the angle α.

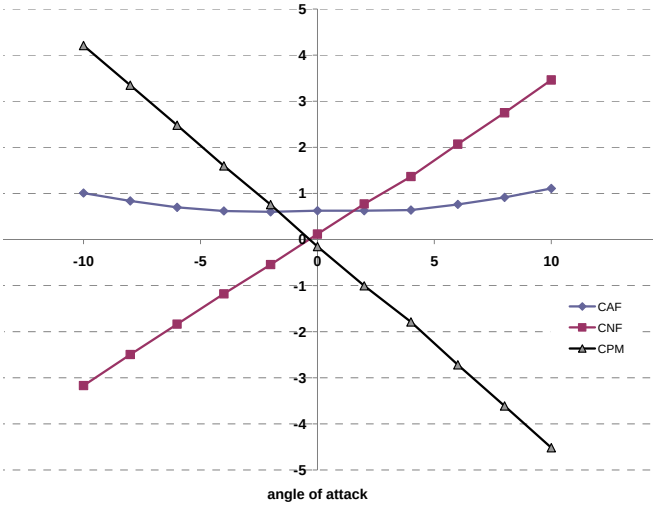

Fig. 8. Values of C_{AF}, C_{NF} and C_{PM} versus angle of attack.

The intermediate measurement precision of the tests was also verified [5]. The changed conditions include disassembling and reassembling the same model in the test section to replicate the whole set of tests. The comparison of the two data sets for the lift force component C_{NF} is presented in Figure 9. The configuration is for the model with null fins deflection. Linear curves were fitted to the data and the deviation between them was considered acceptable.

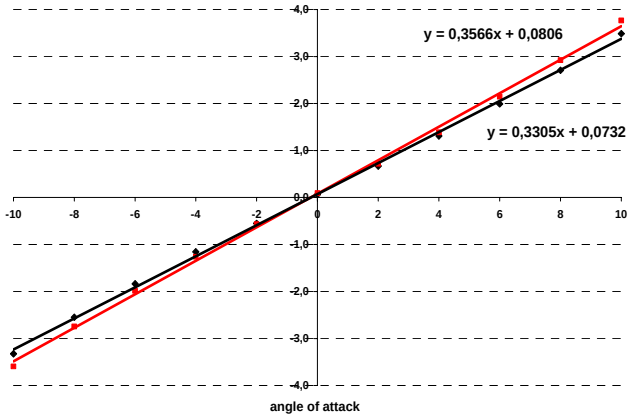

Fig. 9. Analysis of intermediate precision of the tests. Lift component C_{NF}.

The deflection of the fins causes a rolling moment C_{MR} on the vehicle. This behavior is presented in Fig. 10. At 0^o of deflection, the C_{MR} is approximately null and increases with the fin deflection.

There is a compromise between the rolling moment C_{MR} and the axial force coefficient C_{AF}. The drag tends to increase if the rolling moment is high (Fig. 11).

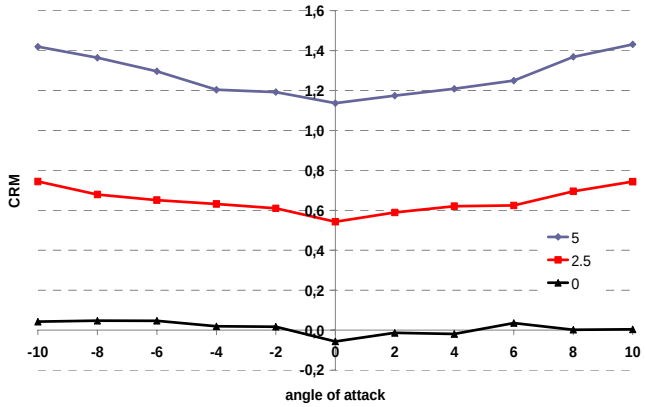

Fig. 10. The influence of the fin deflection on the rolling moment.

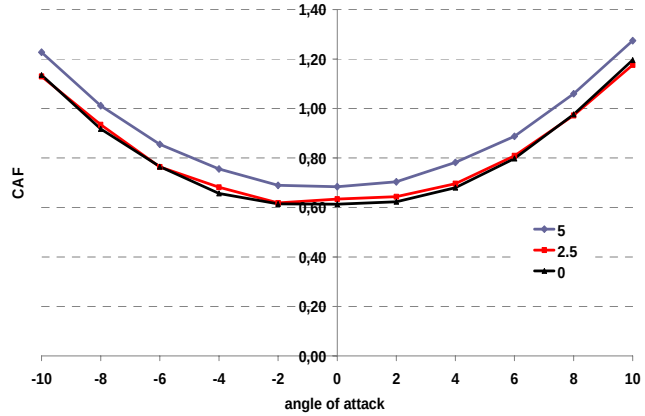

Fig. 11. An increase of the rolling moment C_{RM} causes an increasing in the axial force component C_{AF}.

5. CONCLUSIONS

From this study it was possible to estimate the force and moment aerodynamic coefficients of the Sonda III model, tested for low Mach number in the Pilot Transonic Wind Tunnel of the Institute of Aeronautics and Space.

The aim of the tests carried out was to provide insight on the methodology to be used in the future tests. The test campaign of the Sonda III is still in progress which includes full Mach number transonic range with test of several configurations of the model.

For the Mach number considered in this study, the load coefficients values behave as predicted in the scientific literature.

So far, the most important contribution to the uncertainty in the load components is the measurement precision of the temporal acquisition, evaluated as a type A uncertainty. The

dispersion of the signal is in part due to the injection system, which is not able to supply a more stable flow.

ACKNOWLEDGMENTS

The authors would like to express their gratitude to CNPq, The Brazilian National Council of Research and Development, for the partial funding of this research, under Grant n.º 104775/2008-4.

REFERENCES

[1] M. L. C. C. Reis, R. M. Castro, J. B. P. Falcão, I. M. Barbosa, O. A. F. Mello, "Calibration Uncertainty Estimation for Internal Aerodynamic Balance", XII IMEKO TC1&TC7 Joint Symposium, Annecy, France. Sep 2008.

[2] J. D. Anderson Jr., *Fundamentals of Aerodynamics*, McGraw-Hill, 1984.

[3] J. D. Anderson Jr., *Introduction to Flight*,McGraw-Hill, 3rd ed., 1985.

[4] BIPM, "Guide to the Expression of Uncertainty in Measurements", 1995.

[5] Joint Committee for Guides in Metrology, JCGM 200, "International vocabulary of metrology – Basic and general concepts and associated terms (VIM)", 2008.

[6] Bao-Feng Ma, Xue-Ying Deng, Ying Chen, "Effects of Forced Asymmetric Transition on Vortex Asymmetry Around Slender Bodies", AIAA Journal, Vo. 45, No 11, November 2007.

[7] Bridges, D., "The Asymmetric Vortex Wake Problem – Asking the Right Question", AIAA-2006-3553, 36th AIAA Fluid Dynamics Conference and Exhibit, CA, June 2006.

[8] Hall, R. M., "Influence of Reynolds number on forebody side forces for 3.5-diameter tangent-ogive bodies", AIAA-1987-2274, 5th AIAA Applied Aerodynamics Conference, CA, USA, Aug. 1987.

[9] Soviero, P. A. O., "Modeling of Aerodynamic and Thermodynamic Fields Using the Singularities Method" (Modélisation de Champs Aérodynamique et Thérmique par la Méthode des Singularités), Thèse de docteur-ingénieur, Université Paul Sabatier de Toulouse, 1983.

[10] Hunt, B. L, "Asymmetric Vortex forces and wakes on slender bodies", AIAA-1982-1336, 9th AIAA Atmospheric Flight Mechanics Conference, CA, USA, Aug. 1982.

[11] Hunt B. L., Lamont, P. J., "Comment on Induced Side Forces at High Angles of Attack", Journal of Spacecraft and Rockets, 0022-4650, Vol. 14, No. 5, pp. 319-320, doi: 10.2514/3.57202, 1977.

[12] H. Schilichting, E. Truckenbrodt, H. J. Ramm, *Aerodynamics of the Airplane*, McGraw-Hill, 1979.